increased tunneling current. During metal deposition (Rh, Pd, V, and Al) at room temperature, a regular decoration of antiphase and twin domain boundaries with metal clusters was observed by STM (*1*, *25*), demonstrating their importance as nucleation centers. Furthermore, they serve as diffusion channels for metal atoms from the film surface into the NiAl substrate and could explain how metal clusters disappear from the oxide surface after annealing to higher temperatures (720 K).


**References and Notes**

1. M. Bäumer, H.-J. Freund, *Prog. Surf. Sci.* **61**, 127 (1999).
2. T. Dellwig, G. Rupprechter, H. Unterhalt, H.-J. Freund, *Phys. Rev. Lett.* **85**, 776 (2000).
3. J. S. Moodera, L. R. Kinder, T. M. Wong, R. Meservey, *Phys. Rev. Lett.* **75**, 3273 (1998).
4. N. P. Padture, M. Gell, E. H. Jordan, *Science* **296**, 280 (2002).
5. X. H. Qiu, G. V. Nazin, W. Ho, *Science* **299**, 542 (2003).
6. N. Nilius, N. Ernst, H.-J. Freund, *Phys. Rev. Lett.* **84**, 3994 (2000).
7. K. H. Hansen *et al.*, *Phys. Rev. Lett.* **83**, 4120 (1999).
8. R. Franchy, *Surf. Sci. Rep.* **38**, 195 (2000).
9. J. Libuda *et al.*, *Surf. Sci.* **318**, 61 (1994).
10. G. Binnig, H. Rohrer, Ch. Gerber, E. Weibel, *Phys. Rev. Lett.* **50**, 120 (1983).
11. D. R. Jennison, C. Verdozzi, P. A. Schultz, M. P. Sears, *Phys. Rev. B* **59**, R15605 (1999).
12. D. R. Jennison, A. Bogicevic, *Surf. Sci.* **464**, 108 (2000).
13. Y. Yourdshahyan *et al.*, *J. Am. Ceram. Soc.* **82**, 1365 (1999).
14. S. Ruppi, A. Larsson, *Thin Solid Films* **388**, 50 (2001).
15. Special attention has been devoted to the initial oxidation temperature. Because the amount of Al available to grow an $Al_2O_3$ layer increases rapidly with the initial oxidation temperature, the growth mode and the resulting structure of the oxide layer are strongly dependent on the annealing program.
16. Details of the crystallographic data collection and analysis are available as supporting material on *Science* Online.
17. I. K. Robinson, D. J. Tweet, *Rep. Prog. Phys.* **55**, 599 (1992).
18. A. Stierle *et al.*, data not shown.
19. A. Stierle, F. Renner, R. Streitel, H. Dosch, *Phys. Rev. B* **64**, 165413 (2001).
20. G. Ceballos *et al.*, *Chem. Phys. Lett.* **359**, 41 (2002).
21. M. Kulawik, N. Nilius, H.-P. Rust, H.-J. Freund, *Phys. Rev. Lett.* **91**, 256101 (2003). The authors present a STM-based structural model for the antiphase domain boundaries in agreement with the model proposed in Fig. 3C.
22. K. H. Hansen, T. Worren, E. Laegsgaard, F. Besenbacher, I. Stensgaard, *Surf. Sci.* **475**, 96 (2001).
23. C. L. Pang, H. Raza, S. A. Haycock, G. Thornton, *Phys. Rev. B* **65**, 201401(R) (2002).
24. R. M. Jäger *et al.*, *Surf. Sci.* 259, **235** (1991).
25. M. Frank *et al.*, *Surf. Sci.* **492**, 270 (2001).


**Supporting Online Material**
www.sciencemag.org/cgi/content/full/303/5664/1652/DC1
Materials and Methods
Figs. S1 to S3
Table S1
References and Notes

26 November 2003; accepted 10 February 2004

# Microbial Polysaccharides Template Assembly of Nanocrystal Fibers

**Clara S. Chan,[1]* Gelsomina De Stasio,[2,4]*† Susan A. Welch,[3]‡ Marco Girasole,[5] Bradley H. Frazer,[2,4] Maria V. Nesterova,[3]§ Sirine Fakra,[6] Jillian F. Banfield[1,3]†**

**Biological systems can produce extraordinary inorganic structures and morphologies. The mechanisms of synthesis are poorly understood but are of great interest for engineering novel materials. We use spectromicroscopy to show that microbially generated submicrometer-diameter iron oxyhydroxide (FeOOH) filaments contain polysaccharides, providing an explanation for the formation of akaganeite pseudo–single crystals with aspect ratios of ~1000:1. We infer that the cells extrude the polysaccharide strands to localize FeOOH precipitation in proximity to the cell membrane to harness the proton gradient for energy generation. Characterization of organic compounds with high spatial resolution, correlated with mineralogical information, should improve our understanding of biomineralization mechanisms.**

Organic polymers can play important roles in ecosystems by accumulating biologically important elements. Microbial polymers are known to scavenge iron oxide particles (*1*, *2*) and to induce crystallization of unexpected phases [e.g., nontronite, an iron-rich clay mineral (*3*)]. Organic polymers also act as templates that serve as a pattern for the production of a second structure (*4*), but the templating mechanisms are poorly understood. We report the templation of akaganeite (β-FeOOH) pseudo–single crystals with aspect ratios of ~1000:1 in a natural ecosystem in which extensive microbial biomineralization occurs.

We studied natural biominerals in an iron oxyhydroxide–encrusted biofilm and from overlying groundwater, which was cloudy primarily because of the presence of suspended mineral particles. Samples were collected from flooded (pH 7 to 8.6) underground tunnels of the Piquette Mine, Tennyson, Wisconsin, USA (*5*, *6*). The cloudy water filtrate and biofilm were observed by high-resolution transmission electron microscopy (HRTEM), HRTEM-based energy dispersive x-ray (EDX) spectroscopy, scanning electron microscopy (SEM), and synchrotron-based x-ray photoelectron emission spectromicroscopy (X-PEEM) (*7*). SEM and TEM show that tangled, mineralized filaments are present in the filtrate from the cloudy regions in the water column and underlying biofilm (Fig. 1) (fig. S1). The filaments are typically many micrometers long and range in diameter from 20 to 200 nm. The biofilm also contains ferrihydrite (FeOOH)– and goethite (α-FeOOH)–encrusted sheaths and stalks characteristic of *Leptothrix* spp. and *Gallionella ferruginea* (*8*). In some cases, mineralized filaments and nonmineralizedfibrils appear to extend outward from microbial cells (Fig. 1A) (fig. S2). Thus, we infer that cells extrude polymer strands to localize precipitation reactions. Most filaments were probably attached to cells at one time, but have been shed much like

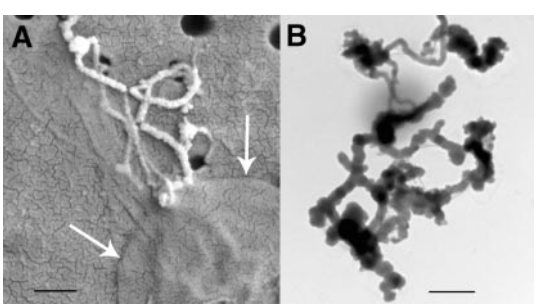


**Fig. 1.** (**A**) SEM image of a cell (edge marked by white arrows) associated with mineralized filaments and nonmineralized fibrils. Scale bar, 0.5 μm. (**B**) TEM image of FeOOH-mineralized filaments filtered from the cloudy water above the biofilm. No crystalline cores are present in these filaments. Scale bar, 0.5 μm.

[1]Department of Earth and Planetary Science, University of California, Berkeley, CA 94720, USA. [2]Department of Physics, [3]Department of Geology and Geophysics, University of Wisconsin, Madison, WI 53706, USA. [4]Synchrotron Radiation Center, Stoughton, WI 53589, USA. [5]Istituto di Struttura della Materia, Consiglio Nazionale delle Ricerche, Rome 00044, Italy. [6]Advanced Light Source, Lawrence Berkeley National Laboratory, Berkeley, CA 94720, USA.

*These authors contributed equally to this work.
†To whom correspondence should be addressed. E-mail: jill@eps.berkeley.edu (J.F.B.), pupa@src.wisc.edu (G.D.S.)
‡Present address: Department of Earth and Marine Sciences, Research School of Earth Sciences, and Cooperative Research Centre for Landscape Environments and Mineral Exploration, Australian National University, Canberra, ACT 0200, Australia.
§Present address: Department of Chemistry and Biochemistry, Montana State University, Bozeman, MT 59717, USA.

*Gallionella* sheds its mineralized stalk (*9*).

Filaments from the cloudy water consist of amorphous iron oxyhydroxide (Fig. 1B). Filaments in the underlying biofilm are morphologically similar, but each contains one thin, pseudo–single crystal core (Fig. 2) surrounded by a porous layer of nanocrystalline 2-line ferrihydrite (Fig. 2D). These cores were observed in all of the ~100 biofilm filaments analyzed by HRTEM. All filaments in the biofilm have essentially the same structure and differ only in the thickness of the ferrihydrite coating and filament length. The pseudo–single crystal fibers at the cores were identified as akaganeite by measurement of lattice fringe spacings and indexing of the Fourier transforms of two HRTEM images in different zone axis orientations (e.g., [−331] zone axis image in Fig. 2C) related by a known tilt angle. Lattice fringe orientations in Fig. 2, B and C, indicate that the tunnels in the akaganeite structure are parallel to the filament length, and that fiber curvature is accommodated by slight misorientations between crystallographically oriented segments of the akaganeite pseudo–single crystal. Akaganeite pseudo–single crystals are about 2 to 3 nm in diameter (parallel to *a* and *c*) and thousands of nanometers in length. The presence of akaganeite is unusual because it is generally considered to form in much higher salinity environments (*10*).

Several lines of evidence suggest that microbial polymers direct the formation of akaganeite in the filaments. Filaments filtered from the cloudy water above the biofilm consist of amorphous FeOOH, which suggests that crystallinity develops upon aging. One akaganeite crystal develops in the core of each individual filament in the biofilm, whereas the remainder of the amorphous iron oxide converts to ferrihydrite (*8*). This indicates that the central region contains a component that controls the aggregation of amorphous FeOOH and then directs mineral structure and orientation over micrometer-length scales.

To verify the presence and nature of organic polymers, we analyzed mineralized filaments and polymer fibrils from the biofilm and cloudy water by X-PEEM (*11*) combined with x-ray absorption near-edge structure (XANES) spectroscopy (Fig. 3) (fig. S3). Iron spectromicroscopy makes it possible to discriminate mineralized filaments and nonmineralized polymer fibrils and to accurately correlate these results with carbon analyses. The carbon K-edge XANES spectrum (Fig. 3C) of nonmineralized fibrils from cloudy water in Fig. 3A matches best with alginate, an acidic polysaccharide, when compared with representative spectra from various organic polymers, including proteins, lipids, and nucleic acids (*12*). Although the spectra from mineralized filaments (images shown in Fig. 3B and fig. S3A, spectra in Fig. 3C and fig. S3C) exhibit a slightly different lineshape, they also match best with the acidic polysaccharide spectrum. Identification of components by XANES spectrum matching depends on how well the standard compounds represent the content of the sample analyzed, hence our interpretation is not unequivocal. However, on the basis of these analyses, we suggest that polysaccharides constitute a significant portion of the organics in each filament and that they are the mineral structure–directing components.

The differences between spectra from mineralized filaments and nonmineralized fibrils may be due to effects of the templated akaganeite on the polymer structure. Absorption features above 290 eV in carbon K-edge spectra are generally associated with photoexcited transitions to states that lie in the continuum (*13*). These multiple-scattering features, or shape resonances, are broad if the environment of the C atom is vibrationally or structurally disordered. Finer structure can be expected if the carbon atom or group is bound in a well-defined environment. The observed peak around 292.4 eV in the mineralized filaments is close to the position of the σ* resonance of the C-O bond of carboxylate groups (*14*), which indicates that the polymer may participate in the templation by binding iron to the carboxyl group. This observation is consistent with other work on the interaction between dissolved Fe(III) and polysaccharides [e.g., (*15*)].

The calculated mass of saccharides measured in the core of the looped mineralized filament shown in Fig. 3B is $\sim 10^{-17}$ g, whereas the mass of the whole filament in the analyzed region is $\sim 2 \times 10^{-13}$ g. Although the volume of the whole filament does not correspond to the probed volume, and an accurate concentration measurement is not possible, the spectrum in Fig. 3C shows sensitivity to only $10^{-17}$ g of material.

Fe L-edge XANES spectra (Fig. 4) confirm the TEM observation that much of the iron oxyhydroxide in the filaments is very poorly crystalline or amorphous. Crystallinity determination with Fe L-edge spectroscopy had not been previously performed but is consistent with well-established Fe K-edge spectral behavior (*16*). There is a clear advantage in expanding spectroscopic analysis and interpretation at the transition metal L-edges; these are all in the soft x-ray region (<1000 eV), as are the organically relevant edges (C, N, and O K-edges). Colocalization of physiological and mineral elements is therefore possible.

Mineralization occurs when extracellular polysaccharides come in contact with oxidized iron. We simulated this process by adding dis-

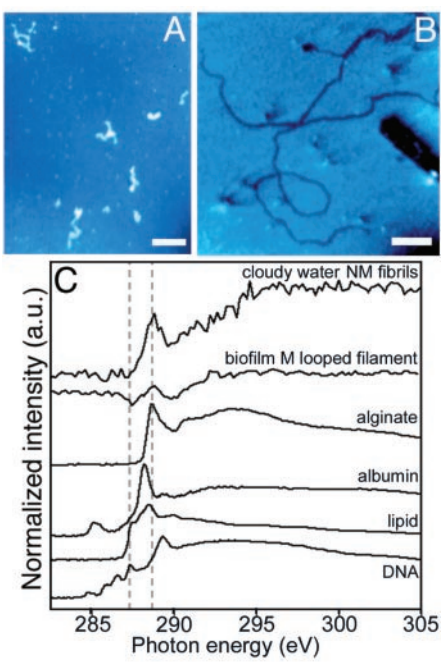


**Fig. 3.** X-PEEM images of (**A**) nonmineralized fibrils from the cloudy water above the biofilm (scale bar, 5 μm) and (**B**) mineralized filaments and a sheath from the biofilm (scale bar, 1 μm). (**C**) Carbon K-edge XANES spectra from multiple nonmineralized (NM) fibrils in (A), the single, looped, mineralized (M) 100-nm-wide filament in (B), and reference organic molecules [from (*12*)]: sodium alginate (acidic polysaccharide), albumin (protein), calf thymus DNA, and 1-palmitoyl-2-hydroxy-*sn*-glycero-3-phosphocholine (a single-chain C-16 saturated lipid). The dashed lines at 287.3 and 288.6 eV highlight the energy position of the most characteristic peaks for DNA and alginate. Notice the similarity of the spectrum from the NM fibrils and the polysaccharide spectrum, and the additional structure in the spectrum from the M filament (peak centered around 292.4 eV). See also fig. S3.

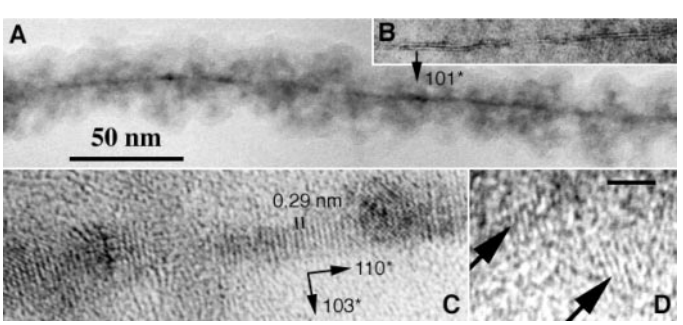


**Fig. 2.** HRTEM images of natural FeOOH-mineralized filaments from the biofilm. (**A**) A filament showing overall structure of thin akaganeite core surrounded by amorphous and finely crystalline iron oxyhydroxide. (**B**) Akaganeite at the filament core. The 0.75-nm (101) lattice fringes are parallel to the filament length. (**C**) [–331] zone axis HRTEM image of akaganeite showing slight misorientations between nanocrystal segments. (**D**) Ferrihydrite nanoparticles (diameter ~2 nm) surrounding the akaganeite core. Scale bar, 1.8 nm.

solved ferric iron to an alginate solution. Scanning transmission x-ray microscopy (STXM) images of the products show thin, long filaments that resemble the natural filaments in size and morphology (Fig. 5A) (fig. S4). Spectral analysis confirms that these filaments contain iron and carbon. Thus, iron oxyhydroxide mineralization of polysaccharide strand templates is a possible explanation for the formation of elongate mineralized structures in nature.

We also tested the hypothesis that self-assembled polysaccharide fibrils can template akaganeite formation. We used a mixture of appropriate polysaccharides with excess carboxylic groups (fig. S5), as expected for metal-binding microbial polymers. After mineralization, HR-TEM observations showed that, as in the natural samples, akaganeite crystals formed within the fibrils (Fig. 5B). The akaganeite crystals displayed microstructure and morphology similar to those of biological origin. Specifically, akaganeite occurs as pseudo–single crystals, each composed of a single chain of aligned nanocrystals. The aspect ratios of the pseudo–single crystals are about 1:25:1; those of the individual nanocrystals are about 1:2:1 to 1:4:1. The smaller aspect ratio of the synthetic akaganeite relative to the natural akaganeite fiber may be attributed to differences between the structures of synthetic fibrils and biological polymer strands, or to differences in reaction rates.

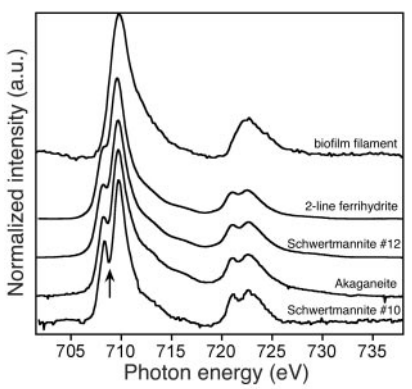


**Fig. 4.** X-PEEM Fe L-edge XANES spectra of the FeOOH mineralized looped filament shown in Fig. 3B, compared with iron oxyhydroxide standards, arranged (bottom to top) in order of decreasing crystallinity, as measured by x-ray diffraction peak broadening. Crystalline phases have well-resolved peaks at ~708.4 and ~709.8 eV. As crystallinity decreases, the dip separating peaks (arrow) decreases in depth. In the mineralized filament, the lack of dip can therefore be interpreted as amorphous iron oxyhydroxide. The Fe spectra from the NM fibrils of Fig. 3A are flat (not shown), indicating that they are not mineralized.

Why would a microbe produce polymer strands, have them mineralized, and then discard them? A conventional argument is that microbes such as neutrophilic iron oxidizers need a mechanism to prevent cell entombment by mineral metabolic byproducts. In this scenario, the precipitates are collected by extruded polymers that are later shed. However, polymer-localized mineral precipitation may have another advantage. Oxidation of iron immediately outside the cell surface is coupled to reduction of oxygen and consumption of a proton at an oxidase on the inside of the cytoplasmic membrane. The oxidation of each $Fe^{2+}$ in solution generates two protons, acidifying the microenvironment adjacent to the membrane:

$$Fe^{2+} + 2H_2O \rightarrow Fe(OH)_2^{+} + 2H^{+} \quad (1)$$

Ferric iron precipitation as iron oxyhydroxide on freshly produced polymers can release protons, which further decrease the pH outside the cell membrane. At neutral and acidic pHs (e.g., pH 5), the dominant aqueous Fe(III) species is $Fe(OH)_2^{+}$ (*17*), which, upon precipitation, releases another proton:

$$Fe(OH)_2^{+} \rightarrow FeOOH + H^{+} \quad (2)$$

In addition, ferrous iron adsorbs onto iron oxyhydroxide surfaces, which catalyze iron oxidation (*18*). Localizing this reaction also decreases the pH near the cell membrane.

The net effect is to increase the pH gradient across the cell membrane by 2 to 4 $H^{+}$ per ferrous iron oxidized, depending on whether the reaction is surface- or enzyme-catalyzed. A diagram of this model is shown in fig. S6. Proton generation localized near the cell wall enhances the proton motive force, thereby increasing the energy-generating potential of the cell. For example, a decrease of 2 pH units across the proton-pumping adenosine triphosphate (ATP) synthases in the cell membrane contributes an increase of ~110 mV to the proton motive force (*19*). We predict that ATP synthases in iron-oxidizing bacteria are located in close proximity to sites of polymer secretion, and that polymer strand production is most prevalent in neutral or alkaline pH environments.

Microorganisms appear to produce polymers that template the growth of extraordinarily long, curved pseudo–single crystals of akaganeite. We infer that the purpose of polymer production is to localize iron oxyhydroxide mineral precipitation in order to enhance metabolic energy generation. Thus, mineral precipitation can be an important determinant of microbial activity levels in the environment. Spatially resolved analyses of organic compounds combined with high-resolution mineralogical information should enhance our understanding of biomineralization mechanisms and promote the development of templation models for use in the fabrication of new materials.

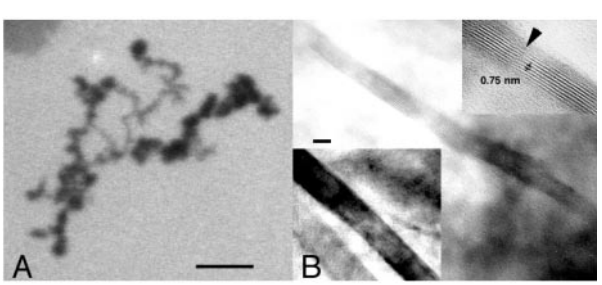


**Fig. 5.** (**A**) STXM image of mineralized filament synthesized in an alginate solution, taken at 300 eV, near the C K-edge. Scale bar, 1 μm. (**B**) TEM image of high aspect ratio akaganeite crystals grown on the polysaccharide gel matrix. The top inset shows two nanoparticle subunits (arrowhead indicates junction) within the pseudo–single crystal. All lattice fringe spacings are 0.75 nm. Scale bar, 6 nm.


**References and Notes**

1. E. G. Sogaard, R. Medenwaldt, J. V. Abraham-Peskir, *Water Res.* **34**, 2675 (2000).
2. D. Mavrocordatos, D. Fortin, *Am. Mineral.* **87**, 940 (2002).
3. M. Ueshima, K. Tazaki, *Clays Clay Miner.* **49**, 292 (2001).
4. S. Mann, *Biomineralization: Principles and Concepts in Bioinorganic Materials Chemistry* (Oxford Univ. Press, Oxford, 2001).
5. M. Labrenz *et al*., *Science* **290**, 1744 (2000).
6. G. K. Druschel, M. Labrenz, T. Thomsen-Ebert, D. A. Fowle, J. F. Banfield, *Econ. Geol. Bull. Soc. Econ. Geol.* **97**, 1319 (2002).
7. See supporting data on *Science* Online.
8. J. F. Banfield, S. A. Welch, H. Zhang, T. T. Ebert, R. L. Penn, *Science* **289**, 751 (2000).
9. H. L. Ehrlich, *Geomicrobiology* (Dekker, New York, ed. 3, 1996).
10. R. M. Cornell, U. Schwertmann, *The Iron Oxides: Structure, Properties, Reactions, Occurrences and Uses* (VCH, Weinheim, Germany, 1996).
11. B. H. Frazer, M. Girasole, L. M. Wiese, T. Franz, G. De Stasio, *Ultramicroscopy,* in press.
12. J. R. Lawrence *et al*., *Appl. Environ. Microbiol.* **69**, 5543 (2003).
13. J. Stöhr, *NEXAFS Spectroscopy* (Springer-Verlag, Berlin, 1992).
14. I. Ishii, A. P. Hitchcock, *J. Chem. Phys.* **87**, 830 (1987).
15. S. J. J. Debon, R. F. Tester, *Food Chem.* **73**, 401 (2001).
16. J. M. Combes, A. Manceau, G. Calas, *Physica B* **158**, 419 (1989).
17. Speciation was modeled using PHREEQC (Version 2) by D. L. Parkhurst and C. A. J. Appelo (U. S. Geological Survey, 1999).
18. B. Wehrli, in *Aquatic Chemical Kinetics*, W. Stumm, Ed. (Wiley, New York, 1990), pp. 311–336.
19. D. G. Nicholls, S. J. Ferguson, *Bioenergetics* (Academic Press, London, ed. 3, 2002).


20. Supported by a National Defense Science and Engineering Graduate Fellowship (C.S.C.), a Consiglio Nazionale delle Richerche Short Term Mobility Fellowship (M.G.), the NASA Astrobiology Institute, and the U.S. Department of Energy (DOE). G.D.S. thanks the University of Wisconsin (UW) Graduate School and Department of Physics for acquisition of the SPHINX microscope. SEM and TEM were performed at the UW Materials Science Center and the EM Lab at the University of California, Berkeley; X-PEEM was performed at the UW Synchrotron Radiation Center (supported by NSF grant DMR 0084402). The Advanced Light Source and work on Beamline 11.0.2 STXM is supported by the Office of Basic Energy Sciences, Division of Materials Sciences, and Division of Chemical Sciences, Geosciences, and Biosciences of the DOE at Lawrence Berkeley National Laboratory under contract DE-AC03-76SF00098. We thank A. P. Hitchcock for making the spectra files of (*12*) available to us, G. Waychunas for providing the akaganeite and schwertmannite standards, T. Araki and M. Gilles for their help in acquiring an alginate spectrum on Beamline 5.3.2, and B. Gilbert for his help and routines for carbon spectra normalization.


**Supporting Online Material**

www.sciencemag.org/cgi/content/full/303/5664/1656/DC1
Materials and Methods
Figs. S1 to S6
References

1 October 2003; accepted 15 January 2004